JOURNAL OF AIRCRAFT
Vol. 30, No. 1, Jan.–Feb. 1993

Fountain Flows Produced by Multijet Impingement on a Ground Plane

J. M. M. Barata*
Instituto Superior Técnico, 1096 Lisbon, Portugal

A numerical and experimental study is made of the characteristics of three-dimensional fountain flows generated by the impingement of two- or three-axisymmetric turbulent jets on a ground plane through the influence of a low-velocity crossflow. This study provides a basis to understanding more complex flowfields in numerous practical situations including jet-powered vertical/short takeoff and landing (V/STOL) aircraft. The simulations are based on the solution of the time-averaged Navier-Stokes equations and the k-ε turbulence model. The computed results are compared with laser-Doppler measurements and visualization results for the cases of two and three jets impinging on a flat plate located at five jet diameters from the jet exit, and a velocity ratio between the jet and crossflow of 30. Comparisons between experimental and numerical results show generally good agreement for the mean flowfield quantities.

Nomenclature

C_1, C_2, C_μ = constants in turbulence model
D = diameter of the jet
G = rate of generation of turbulent kinetic energy
H = height of the crossflow channel
k = turbulence kinetic energy
L = distance between the center of the jets along longitudinal direction
Re = Reynolds number
S = distance between the center of the jets along transverse direction
S_ϕ = source of dependent variable ϕ
S_P^ϕ, S_U^ϕ = components of linearized source term
U = horizontal velocity, $\bar{U} + u'$
V = vertical velocity, $\bar{V} + v'$
X = horizontal coordinate (positive in the direction of crossflow)
X_F = fountain origin
Y = vertical coordinate (positive in the direction of the jet flow)
Z = transverse coordinate (positive on right side of crossflow duct looking upstream)
Γ_ϕ = transport coefficient of dependent variable ϕ
δ_{ij} = kronecker delta
ε = dissipation rate of k
ν = kinematic viscosity
σ_F = jet inclination angle, 90 deg defined as vertical
$\sigma_{k,\varepsilon}$ = Prandtl/Schmidt numbers for k and ε
ϕ = dependent variable ϕ

Subscripts
F = upwash fountain flow
j = jet-exit
o = crossflow
s = stagnation

Received March 9, 1991; presented as Paper 91-1806 at the AIAA 21st Fluid Dynamics, Plasma Dynamics, and Lasers Conference, Honolulu, HI, June 24–26, 1991; revision received Oct. 18, 1991; accepted for publication Dec. 21, 1991.

*Assistant Professor, Mechanical Engineering Department, Av. Rovisco Pais. Member AIAA.

I. Introduction

THE flow of multiple jets issuing into a crossflow is of interest in many practical situations, including smokestacks, sewage outfalls, and jet-powered vertical/short takeoff and landing (V/STOL) aircraft. In this latter application the impingement of each downward-directed jet on the ground results in the formation of a wall jet which flows radially from the impinging point along the ground surface. The interaction of this wall jet with the freestream results in the formation of a ground vortex far upstream of the impinging jet, which has profound aerodynamic implications on the aircraft design (e.g., Barata et al.[1] and Knowles and Bray[2]). In addition, the collision of wall jets originates a fountain upwash flow (Fig. 1), affecting the forces and moments induced on the aircraft when operating in ground effect. Therefore, the successful development of efficient V/STOL aircraft technology requires the knowledge of these flowfields. The objective of this work is the development and validation of a computational method based on the solution of the time-averaged Navier-Stokes equations and the k-ε turbulence model. The method is then used to investigate phenomena that can occur in V/STOL aircraft flowfields.

Earlier detailed measurements of the flow properties of fountain upwash are scarce and have been presented essentially in the absence of crossflow and with the use of probe techniques. The most relevant works have been reviewed by Saripalli[3] and indicated high-turbulence levels and spreading rates in the fountains, e.g., Kind and Suthanthiran[4] and Gilbert.[5] Different interpretations of the measurements have been

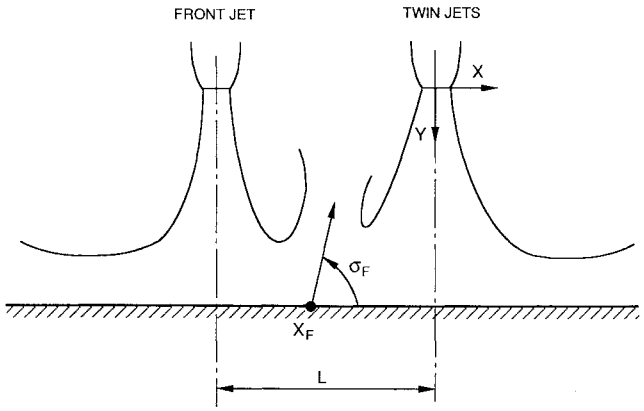

Fig. 1 Schematic of fountain flow.

presented due to the difficulties in measuring complex flows using hot-film and pitot-probe techniques, e.g., Jenkins and Hill[6] and Kotansky and Glaze.[7] Kavasaoglu et al.[8] and Schetz et al.[9] also present flowfield and pressure data for twin-rectangular jets for small jet-to-crossflow velocity ratios (V_j/U_0 = 2.2, 4, and 8). Saripalli[3] reports laser Doppler velocity (LDV) measurements, including those of shear stress, for axisymmetric impinging jets with S/D = 9 and 14 and H/D = 3 and 5.5, but again the existence of a crossflow was not considered.

Reported calculations on these kind of flows have concentrated on the single jet and unconfined problem, and on large impinging distances H, and on very low-velocity ratios V_j/U_0 < 10. Jones and McGuirk[10] did report some calculations on impinging jets in confined crossflow obtained with a finite-difference method, but little attention was given to the strongly impinging case. Childs and Nixon[11] presented calculations relevant to the V/STOL problem using the k-ε model and confirmed the gross features of the flow, but little comparison was given against experimental data to enable a quantitative judgment of the calculations. Schetz and Oh[12] used a finite-element algorithm to study the flow produced by single- and dual-jets issued perpendicular to a flat plate into a crossflow at a velocity ratio of V_j/U_0 = 4, and most of the important features of the surface pressure distribution are well predicted. Barata et al.[1] have also reported numerical calculations for a single jet configuration providing an examination of the computational method based on their detailed measurements. The results are extended in the present work to multijet impinging configurations producing fountain upwash flows, which are the heart of the complicated effects experienced by V/STOL aircraft when they operate in ground proximity.

The next section describes the experimental method, gives details of the flow configuration, laser Doppler velocimeter, and errors incurred in the measurements. Section III describes the mathematical model and Sec. IV presents and discusses the results. The final section summarizes the main findings and conclusions of this work.

II. Experimental Method

A. Flow Configuration

The experiments were carried out in a horizontal water channel, 1.50-m long and 0.5-m wide, made of perspex, as shown schematically in Fig. 2 and described in detail by Barata.[13] The apparatus was built to allow multijet impingement experiments with variable impinging distances H, but in the present study two and three jets of 20-mm exit diameter have been used at a fixed impingement height of 5 jet diameters. The crossflow duct extends 20 D upstream and 55 D downstream of the central upstream jet. For the two-jets configuration the jets are separated by 5 D, (see Fig. 2), and are located 10 D from the nearest sidewall. The third jet center was located at the symmetry plane 15 D far upstream. Each jet unit is comprised of a nozzle with an area contraction ratio

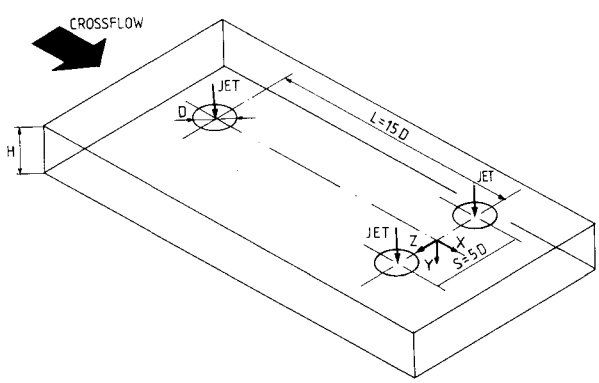

Fig. 2 Diagram of flow configuration.

of 16 and a settling chamber 0.56-m long, which begins with a 7-deg flow distributor followed by flow straighteners. The facility has a recirculating system where both jet and crossflow water are drawn from a discharge tank and pumped to a constant-head tank or supplied to each jet unit by way of control valves. The uniformity of the crossflow was ensured by straighteners and screens.

The origin of the X and Y coordinates is taken at the center of the twin jets, in the upper wall of the tunnel: X is positive in the crossflow direction and Y is positive vertically downwards.

The present results were obtained for Reynolds numbers based on the jet exit conditions of Re_j = 105,000 for a jet-exit mean velocity of 5.1 m/s and a local turbulence intensity of 2% and a crossflow of U_o = 0.17 m/s.

B. Experimental Techniques and Measurement Procedure

The velocity field was measured by a conventional dual-beam, forward-scatter laser velocimeter which was comprised of an argon-ion laser operated at a wavelength of 514.5 nm and a nominal power of 1 W. Sensitivity to the flow direction was provided by light-frequency shifting from acousto-optic modulation (double Bragg cells), a 310 nm focal length transmission lens and forward-scattered light collected by a 150 mm focal lens at a magnification of 0.76. The half-angle between the beams was 3.48 deg (in water) and the calculated dimensions of the measuring volume at the e^{-2} intensity locations were 2.225 and 0.135 mm. The U and V mean and turbulent velocity components were determined by a non-commercial frequency counter interfaced with a microprocessor. The fluctuating velocity components were also used, together with those at 45 deg, to compute the local shear-stream distribution, $\overline{u'v'}$.

Errors incurred in the measurement of velocity by displacement and distortion of the measuring volume to refraction on the duct walls, and the change in refractive index were found to be negligibly small and within the accuracy of the measuring equipment. No corrections were made for sampling bias, and the systematic errors that could have arisen were minimized by using high-data rates in relation to the fundamental velocity fluctuation rate, as suggested by Dimotakis[14] and Erdmann and Tropea.[15] Nonturbulent Doppler broadening (systematic) errors due to gradients of mean velocity across the measuring volume (e.g., Durst et al.[16]), may essentially affect the variance of the velocity fluctuations, but for the present experimental conditions they are sufficiently small for their effect to be neglected. The maximum error is of the order of 10^{-4} V_j^2 and occurs at the edge of the jet. Transit broadening has been shown by Zhang and Wen[17] to be the principal source of error in laser velocimetry. For the present optical configuration the related signal-to-noise ratio is about 69 and the maximum error in the variance of the velocity fluctuations is of the order of 2×10^{-3} V_j^2.

The number of individual velocity values used in the experiments to form the averages was always above 10,000. As a result, the largest statistical (random) errors were 1.5 and 3%, respectively, for the mean and variance values, according to the analysis of Yanta and Smith[18] for 95% confidence interval.

Flow visualization experiments were conducted introducing fluorescein-sodium, a fluorescent dye, as the tracer fluid added directly into the jets, or by using air bubbles as tracer particles to produce short streaks on the photograph. Illumination of the flow was achieved by a sheet of light, obtained by spreading a laser beam (Argon-Ion, 2 W at 488 nm) with a cylindrical lens.

III. Mathematical Model

A. Governing Differential Equations

The steady, isothermal three-dimensional flow is governed by the continuity equation and the three momentum equa-

tions. The density is considered to be uniform. The governing differential equations in Cartesian tensor notation are:

Continuity

$$\rho \frac{\partial \bar{U}_i}{\partial X_i} = 0 \tag{1}$$

Momentum

$$\rho \bar{U}_j \frac{\partial \bar{U}_i}{\partial X_j} = -\frac{\partial \bar{P}}{\partial X_i} + \frac{\partial}{\partial X_j}\left(\mu \frac{\partial \bar{U}_i}{\partial X_j} - \rho \overline{u_i' u_j'}\right) \tag{2}$$

where the overbars represent averaged quantities.

The turbulent stresses are related to the velocity by way of a turbulent viscosity μ_T:

$$-\rho \overline{u_i' u_j'} = \mu_T \left(\frac{\partial \bar{U}_i}{\partial X_j} + \frac{\partial \bar{U}_j}{\partial X_i}\right) - \frac{2}{3}\rho k \delta_{ij} \tag{3}$$

The turbulent viscosity μ_T, which is derived from the two-equation k-ε turbulence model (e.g., Launder and Spalding[19]), is expressed as

$$\mu_T = C_\mu \rho k^2/\varepsilon \tag{4}$$

The equations that govern the distribution of the kinetic energy of turbulence k, and its dissipation rate ε, are

$$\rho \bar{U}_i \frac{\partial k}{\partial X_i} = \frac{\partial}{\partial X_i}\left(\frac{\mu_T}{\sigma_k}\frac{\partial k}{\partial X_i}\right) + G - \rho\varepsilon \tag{5}$$

$$\rho \bar{U}_i \frac{\partial \varepsilon}{\partial X_i} = \frac{\partial}{\partial X_i}\left(\frac{\mu_T}{\sigma_\varepsilon}\frac{\partial \varepsilon}{\partial X_i}\right) + (C_1 G - C_2 \rho\varepsilon)\frac{\varepsilon}{k} \tag{6}$$

The quantity G stands for the rate of generation of k by the action of the velocity gradients as is given by

$$G = \mu_T \left(\frac{\partial \bar{U}_i}{\partial X_j} + \frac{\partial \bar{U}_j}{\partial X_i}\right)\frac{\partial \bar{U}_i}{\partial X_j} \tag{7}$$

The turbulence model constants which are used are those indicated by Launder and Spalding[19]:

C_μ	C_1	C_2	σ_k	σ_ε
0.09	1.44	1.92	1.0	1.3

B. Finite Difference Equations

The governing equations constitute a set of coupled partial differential equations which, apart from differences in the source term, are all of the same form:

$$\frac{\partial U\phi}{\partial X} + \frac{\partial V\phi}{\partial Y} + \frac{\partial W\phi}{\partial Z} = \frac{\partial}{\partial X}\left(\Gamma_\phi \frac{\partial \phi}{\partial X}\right) + \frac{\partial}{\partial Y}\left(\Gamma_\phi \frac{\partial \phi}{\partial Y}\right) + \frac{\partial}{\partial Z}\left(\Gamma_\phi \frac{\partial \phi}{\partial Z}\right) + S_\phi \tag{8}$$

Table 1 describes the relations representing the source terms S_ϕ for each of the variables ϕ.

The finite-difference equations are obtained by discretization of the transport Eq. (8) for each of the variables ϕ. The discretization method used in this study was explained in detail in Barata et al.,[1] and only a brief description will be given here. It involves the integration of the transport Eq. (8) over an elementary control volume surrounding a central node with a scalar value ϕ_P. The convection terms are evaluated using the QUICK scheme proposed by Leonard[20] which is free from artificial diffusion and gives more accurate solutions than the hybrid scheme.

Table 1 Description of source terms

Equation	ϕ	S_ϕ
U-momentum	$\bar{U}$	$-\frac{\partial P}{\partial X}$
V-momentum	$\bar{V}$	$-\frac{\partial P}{\partial Y}$
W-momentum	$\bar{W}$	$-\frac{\partial P}{\partial Z}$
Turbulent kinetic energy	k	$G - \rho\varepsilon$
Dissipation rate	ε	$C_1\varepsilon\frac{G}{k} - C_2\rho\frac{\varepsilon^2}{k}$

C. Solution Procedure and Boundary Conditions

The solution procedure is based on the widely used SIMPLE algorithm and reported in literature (e.g., Patankar and Spalding[21]). It uses the staggered grid arrangement and a guess-and-correct procedure to solve the problem of obtaining a pressure field so that the solution of the momentum equations satisfies continuity.

The computational domain has six boundaries where dependent values are specified: an inlet and outlet plane, a symmetry plane, and three solid walls at the top, bottom, and side of the channel. The sensitivity of the solutions to the location of the inlet and outlet planes was investigated and their final position is sufficiently far away from the jet so that the influence on the computed results is negligible. At the inlet boundary uniform profiles of all dependent variables are specified from the experimental results. At the outflow boundary the gradients of dependent variables in the axial direction are set to zero. On the symmetry plane the normal velocity vanishes, and the normal derivatives of the other variables are zero. To overcome the requirement of very fine grids adjacent to walls in turbulent flow, "wall functions" are introduced to calculate quantities at grid points that are placed well outside the viscous sublayer (see Launder and Spalding[19]). They take the form of expressions for the wall shear stress from which average production and dissipation of k across near-wall cell may be estimated. This method has become most popular (e.g., Patankar et al.,[22] Jones and McGuirk[10]) and has been applied to a large number of different flows with some success (e.g., Rodi[23]).

IV. Results and Discussion

The numerical predictions presented in this section are compared with LDV measurements and visualization results obtained on the central plane of symmetry for the selected flow configurations characterized by $Re_j = 105{,}000$, $V_j/U_o = 30$, $H/D = 5$, $S/D = 5$, and $L/D = 15$, for the two- and three-jet flows. These test cases were predicted using different meshes with up to 180,000 nodes with nonuniform spacing to get finer spacing near the jet and the upwash. This grid refinement study allowed us to select the $19 \times 38 \times 31$ mesh and the $24 \times 92 \times 39$ mesh that give grid independent results for the two- and three-jet cases, respectively.

For all the flows studied, the results have shown (for each jet) a pattern similar to that of a single impinging jet, comprising an initial potential-core jet region and an impingement region characterized by a considerable deflection of the jets. These become almost parallel to the ground plane and originate a ground vortex far upstream of the impinging jets due to the interaction of the wall jets with the crossflow.

For the two-jet configuration, an upwash fountain flow is formed in the center of the two impinging jets due to the collision of the two radial wall jets as shown in Fig. 3. Figures 3a and 3b identify the upwash flow in the vertical plane of symmetry and show that the upwash directions in this plane are asymmetric, because upstream of the jets, the crossflow increases the angle of inclination of the upwash with respect to the ground plane. Visualization of the flow in the transversal plane containing the center of the two jets has shown

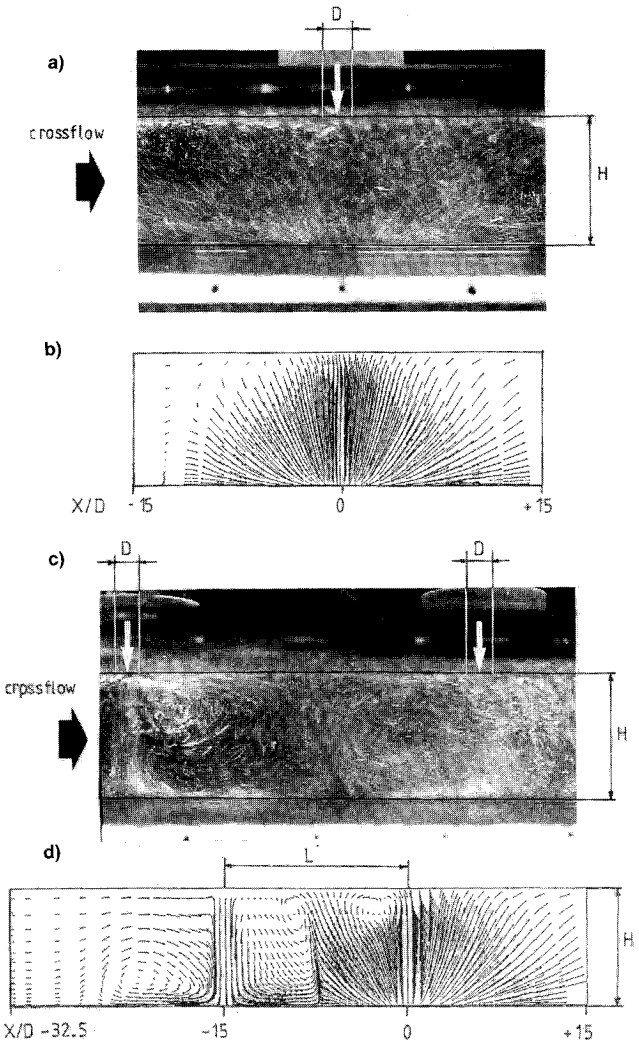

Fig. 3 Experimental and numerical analysis of the fountain upwash flows in the vertical plane of symmetry for Re_j = 105,000, H/D = 5, and V_j/U_o = 30. Two-jet case, S/D = 5: a) flow visualization; b) calculated streak lines over 0.05 s (30 × 60 × 50 mesh), three-jet case, S/D = 5, L/D = 15; c) flow visualization; and d) calculated streak lines over 0.5 s (30 × 120 × 50 mesh).

that the main jets are not strongly affected by the fountain. A considerable entrainment of surrounding fluid into the jets and fountain was observed in a way similar to that described by Saripalli.[3]

In the absence of the crossflow, the wall jets are separated from each other along the ground plane by so-called "stagnation lines" or dividing lines everywhere equidistant from the two-jet impingement centers which contains a stagnation point (e.g., Siclari et al.[24]). In the present case the crossflow originates a second dividing line due to the collision of the wall jets and the crossflow. Near the symmetry plane this line is affected by the interference between the two ground vortexes due to the relatively small jet spacing (S = 5 D).

Figures 3c and 3d show typical experimental and numerical visualization of the flow along the vertical plane of symmetry for the three-jet configuration and identify the "central fountain" which is inclined due to the relative strengths of the jets and crossflow. The inclination of the central fountain as it leaves the ground plane with the X direction derived from Fig. 3c is σ_F = 115 deg. This is the same value obtained by Siclari et al.[24] for three-jet groups without the presence of a crossflow, using a theoretical method based on wall jet momentum equilibrium considerations. The value of σ_F corresponding to the present predictions (Fig. 3d) is about 90 deg, although the fountain inclination increases rapidly to 100 deg at a distance of 1 D from the stagnation point. Siclari et al.[24] use the same theory to estimate additional properties with interest in V/STOL: the fountain origin location and momentum. According to this theory, the fountain origin is located at $X/L = -0.5$ and its momentum is about 16% of the total jet momentum. The experiments show the origin of the fountain located further downstream at $X/L = -0.4$ revealing the influence of the crossflow, whereas the predictions give the value of $X/L = -0.5$. The confinement of the upwash flow and its interaction with the upstream impinging jet gives rise to the recirculation shown in Fig. 3c downstream of the impinging jet, which is present in the calculations but located about 4 D downstream.

Figure 4 shows horizontal profiles of U and V, mean velocity components, and k estimated by $\frac{3}{4}(\overline{u'^2} + \overline{v'^2})$ along the ver-

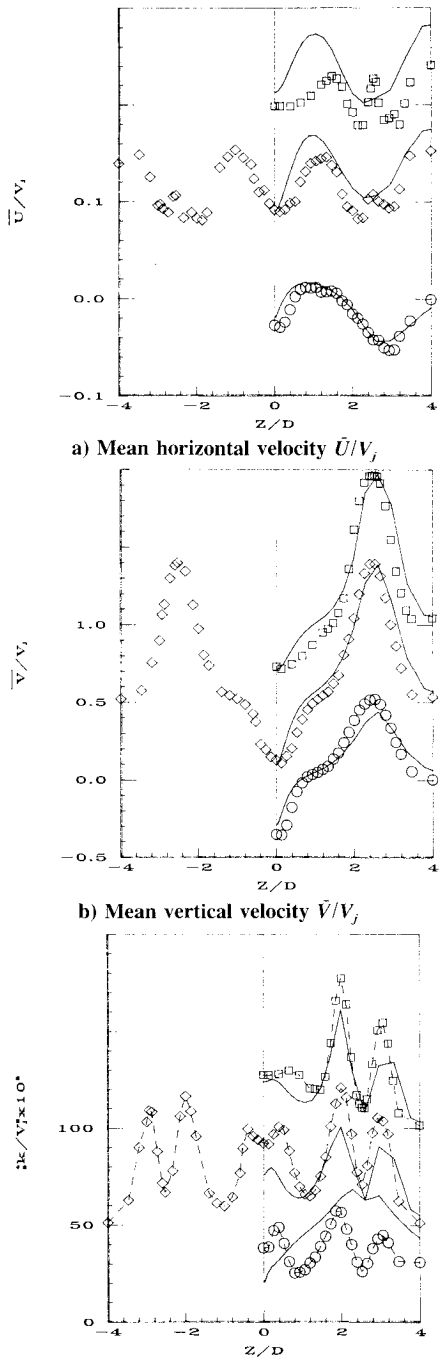

a) Mean horizontal velocity $\bar{U}/V_j$

b) Mean vertical velocity $\bar{V}/V_j$

c) Turbulence kinetic energy $\frac{1}{3}k/V_j^2 \times 10^3$

Fig. 4 Horizontal profiles of velocity characteristics along the vertical transversal plane crossing the center of the jets for the two-jet configuration. Re_j = 105,000, V_j/U_o = 30, H/D = 5, and S/D = 5. Experiments: ○, Y/D = 4.75; ◇, Y/D = 4; □, Y/D = 3; and predictions: ——.

tical plane crossing the center of the jets for the two-jet configuration. The results (particularly those of the vertical velocity component) clearly identify the centrally located fountain rising from the ground. The symmetry of the flow about the central plane between the two jets is also clearly demonstrated in Fig. 4 along the horizontal profiles obtained at $Y/D = 4$. The deflection of the impinging jets by the crossflow is identified close to the ground plate ($Y/D = 4.75$) by the negative values of $\bar{U}$ at the geometrical axis of the jet, i.e., $Z/D = 2.5$. The negative values of $\bar{U}$ at $Z = 0$ are the consequence of the asymmetry of the fountain flow discussed above and indicate that the central stagnation point is displaced downstream by the crossflow. The predicted profiles of $\bar{U}$ and $\bar{V}$ (Figs. 4a and 4b) show a good agreement with the experiments in the impinging jet and upwash flow. The profiles of the turbulent kinetic energy (Fig. 4c) agree qualitatively with the experiments, but the maximum values at the upwash are only well calculated for $Y/D = 3$. For the three-jet configuration (see Fig. 5) similar conclusions can be drawn. The profiles of $\bar{V}$ (Fig. 5b) and k (Fig. 5c) are almost identical, but the $\bar{U}$ profile (Fig. 5a) show negative values at $Z = 0$ and $Y/D = 4$ which were only observed close to the ground for the two-jet configuration.

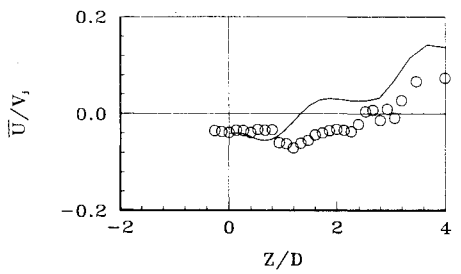

a) Mean horizontal velocity $\bar{U}/V_j$

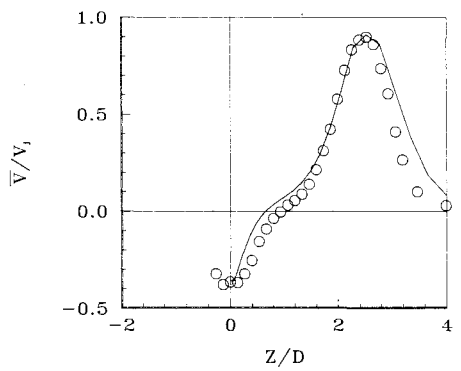

b) Mean vertical velocity $\bar{V}/V_j$

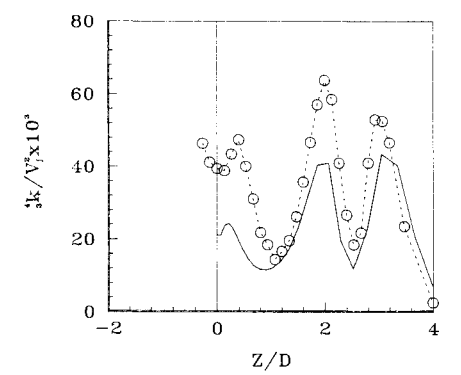

c) Turbulence kinetic energy $\frac{1}{2}k/V_j^2 \times 10^3$

Fig. 5 Horizontal profiles at $Y/D = 4$ of velocity characteristics along the vertical transversal plane crossing the center of the jets for the three-jet configuration. $Re_j = 105{,}000$, $V_j/U_o = 30$, $H/D = 5$, $S/D = 5$, and $L/D = 15$. Experiments: ○; and predictions: ——.

Figures 6 and 7 show horizontal profiles of velocity characteristics along the central plane of symmetry. For the two-jet configuration, the mean horizontal velocities increase in absolute magnitude up to $X/D = \pm 2.7$ and then decline with increased rates closer to the ground plate. The vertical velocities show maximum upward velocities around $X = 0$ and then decline to zero with X. Again, the mean flow values are well predicted although the downstream values are slightly overpredicted indicating a larger asymmetry in the calculations with respect to $X = 0$. Figure 6c confirms the failure of the numerical method to predict the turbulence levels in the upwash flow (at least close to the ground where the flow is subject to strong curvature effects). For the three-jet case (see Fig. 7), the upwash flow around $X = 0$ is similar to that

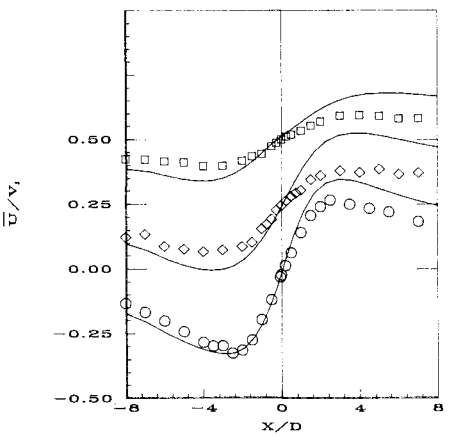

a) Mean horizontal velocity $\bar{U}/V_j$

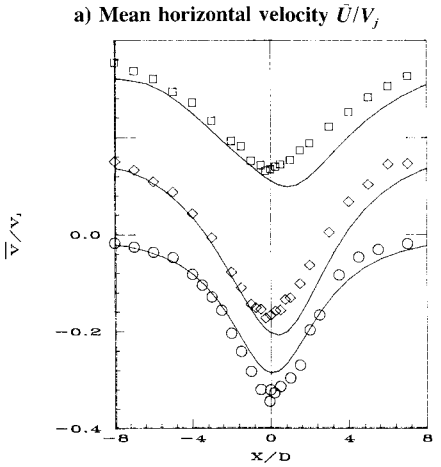

b) Mean vertical velocity $\bar{V}/V_j$

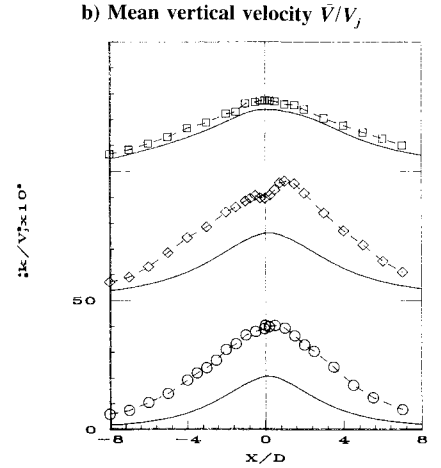

c) Turbulence kinetic energy $\frac{1}{2}k/V_j^2 \times 10^3$

Fig. 6 Horizontal profiles of velocity characteristics along the longitudinal plane of symmetry for the two-jet configuration. $Re_j = 105{,}000$, $V_j/U_o = 30$, $H/D = 5$, and $S/D = 5$. Experiments: ○, $Y/D = 4.75$; ◇, $Y/D = 4$; □, $Y/D = 3$; and predictions: ——.

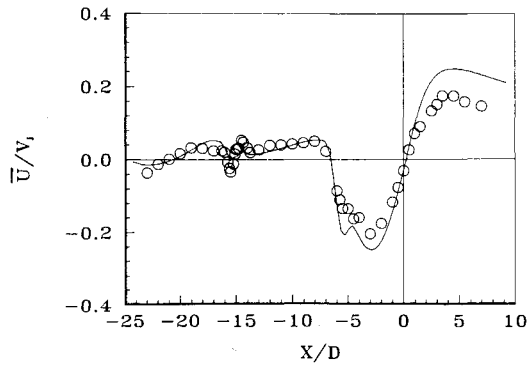

a) Mean horizontal velocity $\bar{U}/V_j$

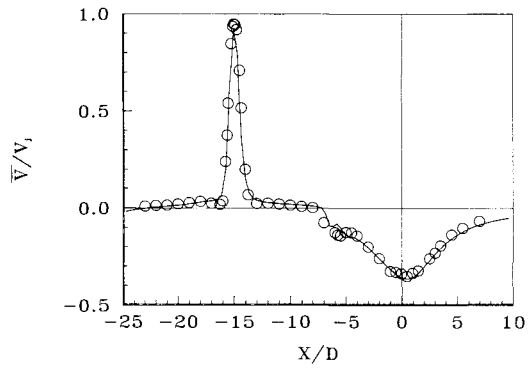

b) Mean vertical velocity $\bar{V}/V_j$

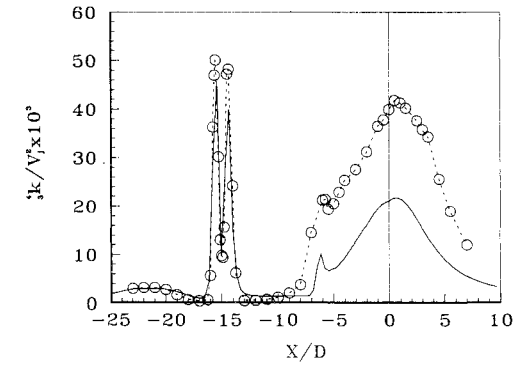

c) Turbulence kinetic energy $\frac{1}{2}k/V_j^2 \times 10^3$

Fig. 7 Horizontal profiles at $Y/D = 4$ of velocity characteristics along the longitudinal plane of symmetry for the three-jet configuration. $Re_j = 105{,}000$, $V_j/U_o = 30$, $H/D = 5$, $S/D = 5$, and $L/D = 15$. Experiments: ○; and predictions: ——.

described previously, although with increased asymmetries. The central fountain upwash flow noted in Fig. 3 is identified between $X/D = -3$ and $X/D = -7$, with a slight increase in the values of the upwards velocity around $X/D = -5$ which is also predicted correctly.

The ability of the computational method to simulate fountain upwash flows was further analyzed through the comparison of the ground-plane pressure distribution for the case of twin jets without crossflow ($H/D = 3$ and $S/D = 6$), obtained by Jenkins and Hill.[6] Figure 8 compares the ground-pressure distributions along the vertical plane crossing the center of the two jets (obtained experimentally by Jenkins and Hill[6]) with the calculated values of Bower[25] and the present work. The present results are very similar to the experimental results in the impinging zone ($0 \leq Z/D \leq 1$), but for $1 < Z/D < 2.5$ it shows slightly negative values which are not detected in the experimental results or in the predictions of Bower.[25] This discrepancy may be attributed to the experimental and numerical difficulties in obtaining very small negative values of static pressure (≈ -0.05). Nevertheless, the existence of

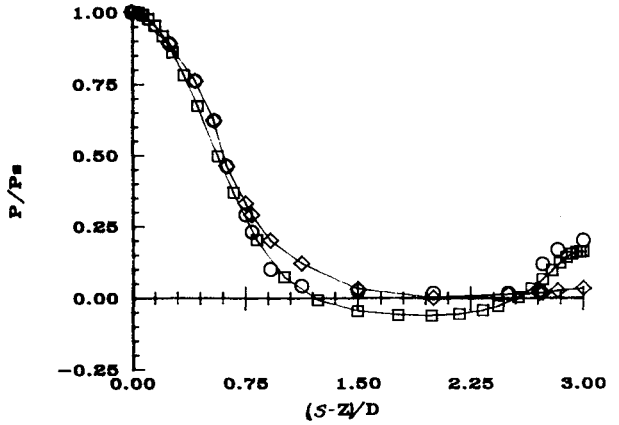

Fig. 8 Ground-plane pressure variation along the vertical plane crossing the center of the two jets for the two-jet configuration. $Re_j = 2 \times 10^5$, $S/D = 6$, and $H/D = 3$. Experiments: ○, Jenkins and Hill[6]; and predictions: ◇, Bower[25]; □, present work.

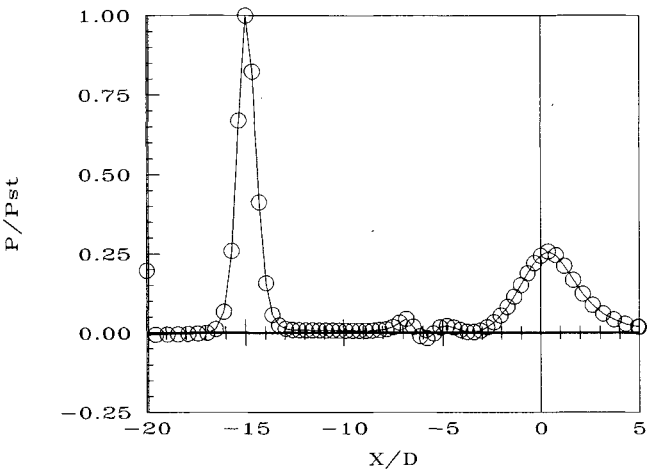

Fig. 9 Ground-plane pressure variation along the vertical plane of symmetry for the three-jet configuration. $Re_j = 105{,}000$, $V_j/U_o = 30$, $S/D = 5$, $H/D = 5$, and $L/D = 15$.

such a negative pressure region is expected for small impinging heights ($H/D < 5$) and was already detected by other authors (e.g., Bower et al.[26] and Barata[13]). In the upwash zone ($2.5 < Z/D < 3$), the present predictions agree quite well with the experimental results and the increase in the fountain pressure can be recognized (which had not been calculated by Bower[25]). This difference can be attributed to the fact that this author used a Reynolds number of 200 which is much lower than the experimental value of Jenkins and Hill[6] of 200,000. Figure 9 presents the calculated ground pressure variation along the symmetry plane for the three-jet flow described above. The results show no significant increase in pressure at the central fountain, while the maximum value at the fountain between the two downstream jets is around 25% of the impinging point value.

Figure 10 shows particle tracks or streak lines of the predicted velocity fields, which clearly shows the ground vortexes due to the interaction between each upstream wall jet and the crossflow. This figure also indicates that a part of fluid of the downstream fountain is captured by each ground vortex (together with fluid from the wall jets), reducing the strength of the central fountain which is associated with the reduction of the pressure values mentioned above. Figure 11 is a three-dimensional perspective of the pressure distribution at $Y/D = 0.8$, showing low-pressure zones with a shape similar to the shape of the ground vortexes. An identical result was found by Barata et al.[1] for the case of single jets with a large low-pressure region resulting from the acceleration of the crossflow over the ground vortex.

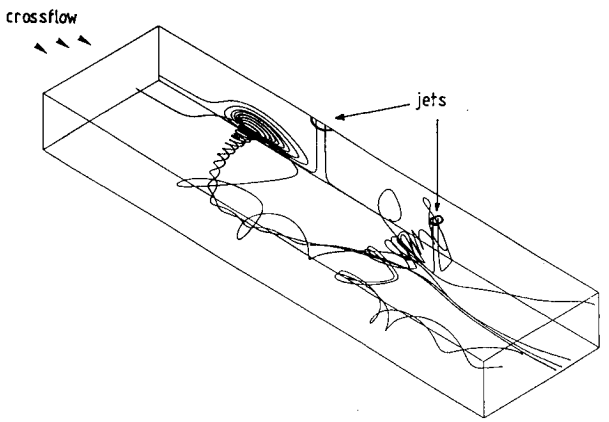

Fig. 10 Calculated three-dimensional streak lines for the three-jet configuration. Re_j = 105,000, V_j/U_o = 30, S/D = 5, H/D = 5, and L/D = 15.

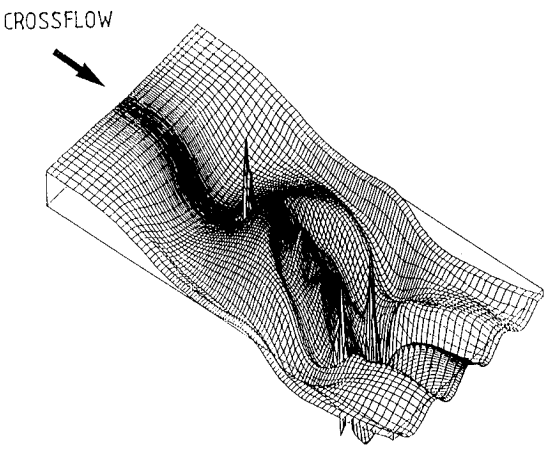

Fig. 11 Predicted three-dimensional perspective of the pressure distribution in a horizontal plane at Y/D = 3.8 for the three-jet configuration. Re_j = 105,000, V_j/U_o = 30, S/D = 5, H/D = 5, and L/D = 15.

V. Conclusions

Laser Doppler measurements have provided information of the mean and turbulent velocity characteristics of the fountain flows produced by two and three round jets impinging on a ground plate through a confined crossflow, for Re_j = 105,000, V_j/U_o = 30, and H/D = 5. The experimental results were used to validate numerical calculations of the flow based on the solution of the finite-difference form of the fully three-dimensional Navier-Stokes equations together the two-equation k-ε turbulence model. The following is a summary of the more important findings of this work.

The experiments have shown a large penetration of the impinging jets which exhibit a similar pattern for two- and three-jet flows. For the latter, a central fountain upwash flow is formed by the interaction between the three-wall jets and is influenced by the downstream ground vortexes which interfere with each other.

Grid independent numerical calculations of the two- and three-jet flows with the Quadratic Upstream Interpolation for Convective Kinematics (QUICK) scheme and the k-ε turbulence model are shown to adequately represent the gross features of the flows. The calculations revealed the existence of large low-pressure regions, already observed in single-jet flows, that for a V/STOL aircraft may produce a substantial negative lift.

References

[1]Barata, J. M. M., Durão, D. F. G., and McGuirk, J. J., "Numerical Study of Single Impinging Jets Through a Crossflow," *Journal of Aircraft,* Vol. 26, No. 11, 1989, pp. 1002–1008.

[2]Knowles, K., and Bray, D., "The Ground Vortex Formed by Impinging Jets in Cross-Flow," AIAA 29th Aerospace Sciences Meeting, AIAA Paper 91-0768, Reno, NV, Jan. 7–10, 1991.

[3]Saripalli, K. R., "Laser Doppler Velocimeter Measurements in 3D Impinging Twin-Jet Fountain Flows," *Turbulent Shear Flows,* Vol. 5, edited by F. Durst et al., Springer-Verlag, Berlin, 1987, pp. 147–168.

[4]Kind, R. J., and Suthanthiran, K., "The Interaction of Two Opposing Plane Turbulent Wall Jets," AIAA Paper 72-211, Jan. 1980.

[5]Gilbert, B. L., "Detailed Turbulence Measurements in a Two Dimensional Upwash," AIAA 16th Fluid and Plasma Dynamics Conf., AIAA Paper 83-1678, Danvers, MA, July 12–14, 1983.

[6]Jenkins, R. C., and Hill, W. G., Jr., "Investigation of VTOL Upwash Flows Formed by Two Impinging Jets," Grumman Research Dept. Rept. RE-548, Bethpage, NY, Nov. 1977.

[7]Kotansky, D. R., and Glaze, L. W., "The Effects of Ground Wall-Jet Characteristics on Fountain Upwash Flow Formation and Development," Rept. ONR-CR212-216-1F, 1980.

[8]Kavsaoglu, M. S., Schetz, J. A., and Jakubowsky, A. K., "Rectangular Jets in a Crossflow," *Journal of Aircraft,* Vol. 26, No. 9, 1989, pp. 793–804.

[9]Schetz, J. A., Jakubowsky, A. K., and Aoyagi, K., "Surface Pressures on a Flat Plate with Dual Jet Configurations," *Journal of Aircraft,* Vol. 21, No. 7, 1984, pp. 484–490.

[10]Jones, W. P., and McGuirk, J. J., "Computation of a Round Turbulent Jet Discharging into a Confined Crossflow," *Turbulent Shear Flows 2,* 1980, pp. 233–245.

[11]Childs, R. E., and Nixon, D., "Simulation of Impinging Turbulent Jets," *Proceedings of the AIAA 23rd Aerospace Sciences Meeting,* AIAA, New York, 1985.

[12]Schetz, J. A., and Oh, T. S., "Finite Element Simulation of Complex Jets in a Crossflow for VSTOL Applications," *Journal of Aircraft,* Vol. 27, No. 5, 1990, pp. 389–399.

[13]Barata, J. M. M., "Experimental and Numerical Study of the Aerodynamics of Impinging Jets in a Crossflow" (in Portuguese), Ph.D. Dissertation, Instituto Superior Técnico, Technical Univ. of Lisbon, Lisbon, Portugal, 1989.

[14]Dimotakis, F., "Single Scattering Particle Laser-Doppler Measurements of Turbulence," AGARD-CP-13, Paper 10.7, 1978.

[15]Erdmann, J. C., and Tropea, C. D., "Turbulence-Induced Statistical Bias in Laser Anemometry," *Proceedings of the 7th Biennal Symposium on Turbulence,* Rolla, MO, 1981.

[16]Durst, F., Melling, A., and Whitelaw, J. H., *Principles and Practice of Laser-Doppler Anemometry,* 2nd ed., Academic Press, New York, 1981.

[17]Zhang, Z., and Wen, J., "On Principal Noise of the Laser Doppler Velocimeter," *Experiments in Fluids,* Vol. 5, 1987, pp. 193–196.

[18]Yanta, W. J., and Smith, R. A., "Measurements of Turbulent-Transport Properties with Laser-Doppler Velocimeter," 11th Aerospace Science Meeting, AIAA Paper 73-169, Washington, DC, 1978.

[19]Launder, B. E., and Spalding, D. B., "The Numerical Computation of Turbulent Flows," *Computer Methods in Applied Mechanics and Engineering,* Vol. 3, 1974.

[20]Leonard, B. P., "A Stable and Accurate Convective Modelling Procedure Based on Quadratic Upstream Interpolation," *Computer Methods in Applied Mechanics and Engineering,* Vol. 19, 1979, pp. 59–98.

[21]Patankar, S. V., and Spalding, D. B., "A Calculation Procedure for Heat, Mass and Momentum Transfer in Three-Dimensional Parabolic Flows," *International Journal of Heat and Mass Transfer,* Vol. 15, 1972.

[22]Patankar, S. V., Basu, D. K., and Alpay, S. A., "Prediction of the Three-Dimensional Velocity Field of a Deflected Turbulent Jet," *Journal of Fluids Engineering,* Vol. 99, Dec. 1977, pp. 758–762.

[23]Rodi, W., "Examples of Turbulence Models for Incompressible Flows," *AIAA Journal,* Vol. 20, No. 7, 1982, pp. 872–879.

[24]Siclari, M. J., Migdal, D., Luzzi, T. W., Jr., Barche, J., and Palcza, J. L., "Development of Theoretical Models of Jet-Induced Effects on V/STOL Aircraft," *Journal of Aircraft,* Vol. 13, No. 12, 1976, pp. 938–944.

[25]Bower, W. W., "Computations of Three-Dimensional Impinging Jets Based on the Reynolds Equations," *Proceedings of the AIAA/ASME 3rd Joint Thermophysics, Fluids, Plasma and Heat Transfer Conference,* AIAA, New York, June 1982.

[26]Bower, W. W., Kotansky, D. R., and Hoffman, G. H., "Computations and Measurements of Two-Dimensional Turbulent Jet Impingement Flowfields," *Proceedings of the 1st Symposium on Turbulent Shear Flows,* University Park, PA, April 18–20, 1977.